Reduction-oxidation Enabled Glass-ceramics to Stainless Steel Bonding Part II, interfacial bonding analysis

Steve Dai

Materials Science and Engineering Center Sandia National Laboratories Albuquerque, NM 87185-1349, USA

Abstract

Among glass-ceramic compositions modified with a variety of oxidants (AgO, FeO, NiO, PbO, SnO, CuO, CoO, MoO₃ and WO₃) only CuO and CoO doped glass-ceramics showed existence of bonding oxides through reduction-oxidation (redox) at the GC-SS interface. The CuO-modified glass-ceramics demonstrate the formation of a continuous layer of strong bonding Cr₂O₃ at the interface in low partial oxygen (PO₂) atmosphere. However, in a local reducing atmosphere, the CuO is preferentially reduced at the surface of glass-ceramic rather than the GC-SS interface for redox. The CoO-modified glass-ceramics demonstrate improved GC-SS bonding. But the low mobility of Co⁺⁺ ions in the GC limited the amount of CoO that can diffuse to and participate in redox at the interface.

Introduction

Lithium silicate glass-ceramics, usually modified with a small amount of other oxides (for example, K_2O , B_2O_3 , Al_2O_3 , ZnO, and often P_2O_5 as the high temperature nucleating agent) have been extensively used for sealing electrical feedthroughs in metal housings [1]. Depending on the type, as well as the amount of the crystallized phases, GCs with a moderate to high coefficient of thermal expansion (CTE) (10 - 18 ppm/ $^{\circ}$ C) can be produced [2,3].

Two patented lithium silicate glass-ceramics, Li₂O-SiO₂-Al₂O₃-K₂O-B₂O₃-P₂O₅ (designated SB glass [4]), and Li₂O-SiO₂-Al₂O₃-K₂O-B₂O₃-P₂O₅-ZnO (designated as belt processable S-glass (BPS) glass-ceramic [5]), were developed to seal electrical feedthroughs to nickel-based and stainless steel (SS) alloys. In particular, high CTE BPS glass-ceramic was developed to form matched hermetic seals to high expansion low-carbon stainless steel, such as 304L (CTE = 18.9 ppm/°C, 40 °C – 600 °C). The high CTE of BPS glass-ceramic was achieved by maximizing the crystallization of high expansion Cristobalite, along with other crystalline phases including nucleant Li₃PO₄, Li₂SiO₃, and a minor amount of Li₂Si₂O₅ and quartz.

For matched GCtSS seals a bonding between the sealing material and metal housing is essential for hermeticity, as opposed to compression seals where the bond is not a necessity. However, despite complex multiple interfacial reactions between the glass-ceramic and the stainless steel [6,7,8,9,10,11], there is no evidence on the existence of a chemical bond, defined as a saturated interfacial oxide adhesion layer that bridges the metallic bonding of steel to the ironic-covalent bonding of glass [1], between the two materials.

In Part I of this series a number of glass-ceramic compositions modified with a variety of oxidants, AgO, FeO, NiO, PbO, SnO, CuO, CoO, MoO₃ and WO₃, are examined for the possibility of forming bonding oxides through reduction-oxidation (redox) at the GC-SS interface. The criteria for a viable modification of glass-ceramic are the following: 1) The oxidant could be reduced, preferably over P₂O₅ in glass-ceramic, to preserve the P₂O₅ to form Li₃PO₄ nuclei as nucleation agents for crystallization of glass--ceramics; 2) The metal ions of the dopants have the mobility to quickly diffuse to the interface; so kinetically, the redox is feasible.

3) The oxidants need to be reduced at the GC-SS interface for redox reaction rather than at the free surfaces of the glass-ceramic.

Among all modified glass-ceramics only those doped with proper amount of CuO and CoO demonstrated bonding to stainless steel. The focus of this paper as Part II of the series is to investigate the bonded GC-SS interface and look for microstructural evidence of interfacial redox reactions. Fractured GC-SS bonds are also examined to reveal failure mechanisms at the interface.

Experiment

Sessile Drop Tests: Cubes diced from ingots of modified glass-ceramics at a size 0.066 x 0.066 x 0.066 inch were placed on stainless steel coupons for wetting and adhesion tests.

<u>GC –SS Bonding Measurements</u>: Stainless steel pins at diameter 0.098 inch and lengths 0.5 or 1.0 inch with a Ra 32 finish on the end surfaces were used for glass-ceramic bonding tests. The bonded glass-ceramic and stainless steel specimens were processed in two forms: a GC-pin

specimen with the glass-ceramic cube sitting on top of the steel pin, and a pin-GC-pin configuration with the glass-ceramic cube sandwiched between two steel pins.

The quantitative measurement of adhesion strength depended on the configuration of the GC-SS sample. For a pin-GC-pin sample, the adhesion pull test was conducted using a standard Instron pull tester. For a GC-pin sample, the glass-ceramics is bonded vertically to a diameter 0.5 x thickness 0.125 inch aluminum disc. A partial spherical dimple was machined at the center of the aluminum disc to accommodate the dome-shaped glass-ceramics. Hysol 9394 2-part epoxy was used to bond the glass-ceramics to the aluminum disc at a curing temperature 150 °C for 2 hours. The assembly was subject to a standard pull test, very much like the test of solder adhesion, that was conducted by the Romulus Universal Materials Tester from Quad Group.

Glass-Ceramic Chemistry and Microstructure Analysis: The analysis of general morphology and element mapping were conducted mostly by scanning electron microscopy (SEM) on glass-ceramics and stainless steels to analyze the reactions zones. Wherever needed, the tunneling technique and electron back scattering diffraction (EBSD) were used in SEM analysis for verification of crystalline phases in glass-ceramics and stainless steels. For detailed study on the interfacial bonding oxide(s), specimens were cut across the bonded GC-SS interface by the focused ion beam (FIB) technique and analyzed by transmission electron microscopy (TEM).

Results and Discussion

1. CoO-modified GCs

The CoO modified glass-ceramics demonstrated acceptable wetting and adhesion to stainless steel (Table 8 in Part I). This section focuses on wetting, bonding and interfacial analysis between the glass-ceramics and stainless steel.

1.1. Sessile drop tests

Figure 1 shows the sessile drop results of four glass-ceramic compositions, BPS_Co1, BPS_Co2, SB_Co1 and SBCo_2. The SB_Co1 wet but did not adhere to the SS (Figure 1a). The SB_Co2 wet and adhered to the SS (Figure 1b), as did both BPS_Co1 and BPS_Co2 (Figure 1c). A close inspection of two CoO doped BPS glass-ceramics (Figure 1d) clearly revealed the existence of a reaction zone. The color of the reaction zone is much lighter than deep blue color of the bulk glass-ceramics and close to that of the original white BPS glass-ceramics, suggesting a depletion of Co⁺⁺ ions in the reaction zones.

It was also found that the adhesion of BPS_Co1 to the stainless steel was weaker than that of the BPS_Co2. Many of the initially adhered BPS_Co1 drops fell off after the samples were handled, while the BPS_Co2 drops stayed bonded all the time. Similarly, the SB_Co2 adhered to the stainless steel well. It appeared that a higher level of CoO doping helped the glass-ceramics' adhesion to the stainless steel.

1.2. Pin bonding tests

An initial experiment was to seal a GC-pin in a graphite fixture. Figure 2 shows the adhesion results of BPS_Co1 and BPS_Co2. The pins did not show any signs of being oxidized, which is consistent with the reducing atmosphere inside the graphite fixture. One of the BPS_Co1 glass-ceramics fell off, while the other stayed on, suggesting that the adhesion is marginal and inconsistent. Both BPS_Co2 glass-ceramics adhered well to the pins. A transmission optical view of BPS_Co2 (Figure 1c) clearly revealed a Co depletion zone in the glass-ceramics near the interface. A noticeable finding was the imperfect dome shape of the glass-ceramic surfaces, suggesting a very viscous flow of glass-ceramic after melting. In sealing, the glass-ceramics may not be able to flow freely and reach an equilibrium shape. Rapid bulk crystallization and/or surface nucleation and crystallization might dramatically change the viscosity locally and attribute to the limited flow of the glass-ceramic. Examinations of both the BPS_Co1 and BPS Co2 glass-ceramics indicated there was no Co migration to the surface of the specimens.

Bonding tests were also conducted on BPS_Co1 and BPS_Co2 using a pin-GC-pin configuration in a graphite fixtures. The BPS_Co1 had a limited adhesion to the pins. The pin-GC-pin assemblies stayed bonded after sealing but broke at the GC-pin interface after minimal handling, leaving shiny end surfaces on the stainless steel pins.

On the other hand, strong bonding of the BPS_Co2 to the pins was observed. Figure 3a shows one bonded pin-BPS_Co2-pin, sample 1, and two fractured samples 2 and 3. Sample 2 was manually fractured to study the failure mode. The fracture occurred through the middle of the glass-ceramic, suggesting that the GC-pin interface was stronger than the glass-ceramic itself. The two fractured glass-ceramic surfaces are shown in Figure 3b. Sample 3 was subjected to a

controlled Instron tensile test. The breaking force was around 19 lb (2420 Psi). The failure appeared to be at one GC-pin interface. A close inspection of the fractured surface on the glass-ceramic showed that small pieces of glass were chipped away. Correspondingly residual glass-ceramic was observed throughout the fractured surface of the stainless steel pin, as shown in Figure 3c. The failure mode in this specimen suggested that the strength of the GC-SS bond is close to the strength of the glass-ceramics. The overall bonding of BPS_Co2 glass-ceramics to stainless steel was significantly improved over the original unmodified BPS glass-ceramic.

1.3. Interfacial reactions of CoO-modified GCs and SS

SEM cross-section image and element maps of BPS_Co2 and stainless steel pin are shown in Figure 4. The key findings are: 1) There is a reaction zone in glass-ceramic next to the interface, characterized by a coarsened crystalline structure compared to the much finer crystalline structure in the bulk glass-ceramic. 2) There is Cr diffusion from stainless steel and the formation of Cr_2O_3 at the GC-SS boundary and in the glass-ceramic. While the Cr_2O_3 in glass-ceramic may not contribute to the adhesion, the Cr_2O_3 at the interface could promote adhesion. There also appears to be metallic Cr in the BPS_Co2 glass-ceramic which was not seen in BPS glass-ceramic. 3) There is P depletion in the glass-ceramic reaction zone and an accumulation of P at the interface. The reduction of P_2O_5 could be a source for oxidation of P_3 could be a course for oxidation of P_3 could contribute to the unnodified BPS GC-SS interface. 4). A reduction of P_3 could be a source for oxidation of P_3 could contribute to the unnodified BPS GC-SS interface. 4). A reduction of P_3 could be a source for oxidation of P_3 could contribute to the unnodified BPS GC-SS interface. 4). A reduction of P_3 could be a source for oxidation of P_3 contribute to the unnodified BPS GC-SS interface. 4). A reduction of P_3 could be a source for oxidation of P_3 contribute to the interface.

It appeared that the intended $3\text{CoO} + 2\text{Cr} \rightarrow 3\text{Co} + \text{Cr}_2\text{O}_3$ redox occurred at the GC-SS interface, and helped the glass-ceramic to stainless steel adhesion. However, the CoO did not shield P_2O_5 from being reduced. The reaction zone in glass-ceramic with a coarse microstructure still existed due to a depletion of P, and thus less LiPO₄ nuclei for crystallization. One of the explanations on the limited role of CoO might be a slow diffusion of the Co⁺⁺ ions in the glass-ceramic, as suggested by the white Co-free region in Figure 1c. It was clear that the majority of Co⁺⁺ in the bulk GC did not migrate in the sealing cycle. Only the Co⁺⁺ ions near the GC-SS interface diffused to participate in the interfacial redox, leaving a distinct colorless Co⁺⁺ free region in glass-ceramic near the interface.

2. CuO-modified Glass-ceramics

Glass-ceramics with 2wt% CuO added were found to form a thin reaction zone and an absence of the phosphate phases in the zone [1]. Bonding was achieved via a thin $(0.2 \sim 0.5 \,\mu\text{m})$ interfacial layer that is rich in Cr. However there was no discussion on whether an interfacial redox occurred and the nature of the bonding layer. The current section attempted to address these issues.

2.1. Sessile drop tests and the effect of sealing atmosphere

Figure 5 shows a sessile drop test in furnace N_2 of four CuO modified SB glass-ceramics, with CuO at 0.25, 0.50, 0.75 and 1.0 mol%. At the lowest amount of 0.25 mol% CuO, the SB_025Cu glass-ceramic wet but did not adhere to the stainless steel. There is slightly reduced Cu seen at the glass-ceramic surface. The SB_050Cu did not wet the stainless steel as well as the SB_025Cu

but seemed bonded to the stainless steel, with significant Cu appearing at the surface. Both SB_075Cu and SB_100Cu adhered to the stainless steel very well with almost no evidence of Cu at the surfaces. Both appeared to be light blue, indicating some residual Cu⁺⁺ ions in the bulk glass-ceramic. As it will become clear in further studies, the majority of the CuO in these compositions participated in the interfacial redox.

It has been shown that the trace oxygen in furnace N₂ affected the wetting of glass-ceramics on stainless steel (see Part I). The effects of the residual oxygen on CuO-doped glass-ceramics were much more profound. Figure 6a shows the sessile drop test of SB_050Cu and SB_100Cu in a graphite box. The stainless steel coupon showed no indication of being oxidized. Both glass-ceramic drops were covered by metallic Cu at the surface and showed no wetting on the stainless steel. Clearly the CuO was reduced at the surface of the glass-ceramics, rather than being reduced at the GC-SS interface. The reduced Cu tended to minimize the surface area of glass-ceramics by forming spherical glass-ceramic beads on the stainless steel.

A sessile drop test on pre-oxidized stainless steel inside a graphite box was also conducted (Figure 6b). The SB_100Cu clearly wet the oxidized stainless steel while the SB_050Cu did not wet the stainless steel at all. Both fell off from the SS without adhesion. Again the presence of Cu at the glass-ceramics' surface suggested that the CuO was reduced at the surface, presumably due to the reducing atmosphere inside a graphite fixture.

The effect of a sealing atmosphere could be summarized as follows: 1) In the presence of trace oxygen, the GC-SS interfacial redox of $3\text{CuO} + 2\text{Cr} \rightarrow 3\text{Cu} + \text{Cr}_2\text{O}_3$ dominated the reduction of

CuO, and the CuO reduction occurred mainly at the interface; and 2) In a reducing atmosphere, the reduction of $2\text{CuO} \rightarrow 2\text{Cu} + \text{O}_2$ at the glass-ceramic surface proceeded over the interfacial redox, and the reduced Cu emerged at the glass-ceramic surface rather than the interface. The findings have important practical implications. The local atmosphere has a significant effect on how CuO is being reduced in CuO modified glass-ceramics. The specific atmosphere associated with a particular fixture material thus directly affects how and where the CuO is reduced in the sealing of CuO modified glass-ceramics to stainless steel.

2.2. GC-SS bonding by interfacial redox

A SEM cross-sectional examination of the SB_100Cu sessile drop sample is shown in Figure 7. The major findings are: 1) Metallic Cu particles at sub-micron size existed in glass-ceramic near the GC-SS interface. There was no or minimum Cu in the bulk glass-ceramic. All Cu⁺⁺ appeared to diffuse towards the interface and accumulated next to the interface. 2). There is a thin (\sim 0.1 μ m) Cr-rich oxide layer between the discrete Cu particles and the stainless steel. Accordingly there is Cr depletion zone in the stainless steel, suggesting an interfacial redox reaction. Most importantly, all Cr depleted from stainless steel appeared to accumulate right at the interface without any indication of Cr diffusion into, and subsequent formation of Cr₂O₃ in, the bulk glass-ceramic. For comparison, the thickness of the bonding oxide layer containing Cr, Mn and Si is \sim 1 μ m [12] in the sessile drop experiment on pre-oxidize austenitic stainless steel.

Two areas of SB_100Cu glass-ceramic, one in the bilk and the other next to the GC-SS interface, were examined for microstructure and P distribution (Figure 8). The two SEM images showed

identical microstructure and crystalline phases. There is no evidence of a reaction zone in glass-ceramic with abnormal crystal growth, as seen in BPS glass-ceramic. Further, the P map showed uniform distribution of P throughout the glass-ceramic, with no indication of a P depletion zone near the interface, again, as seen in the BPS glass-ceramic. The CuO apparently shielded the P_2O_5 in the glass-ceramic from being reduced and served as the preferred oxidant for interfacial redox.

TEM analysis was conducted on a SB_100Cu GC-SS FIB cut sample across the interface. Figure 9 shows an overview of the GC-SS interface with the presence of a Cu particle. EDS (energy dispersive spectroscopy) was used to map elements from a selected area, as indicated by a green box in the TEM image. Observations from TEM data could be summarized as follows. 1) Interfacial oxides. The interfacial oxides appeared to be many individual crystals. One side of the crystals connected to the stainless steel with the rest dispersed in the glass-ceramic. The size of the crystals was 100s nm. 2) No reaction zone in glass-ceramic was observed. 3) There is an obvious reaction zone in the stainless steel, presumably from the depletion of Cr. A similar Cr depletion zone was observed in sessile drop experiment on pre-oxidized stainless steel [13].

As shown in the element maps in Figure 9, the interfacial oxide appeared to be the MnCr₂O₄ spinel as the Mn overlaps well to the presence of Cr. However, further TEM characterization using the selected area electron diffraction (SAED) analysis revealed that the presence of Mn was an artifact due to the proximity of the Mn and Cr peaks in EDS analysis. The SAED patterns from different parts of the sample unambiguously identified the glass phase, the Cu particle and the Cr₂O₃ crystals at the interface by fitting to the related lattice parameters (Figure 10). The Cr

was the main reducing agent from stainless steel to participate in the interfacial redox. The interfacial bonding oxide was Cr_2O_3 .

Figure 11 illustrates the microstructure of the SB_100Cu GC-SS interface as a result of the interfacial redox. Starting from glass-ceramic, the sequence of the materials stack-up can be described as: bulk glass-ceramic \rightarrow glass-ceramic + Cu particles \rightarrow thin layer assembly of Cr_2O_3 crystals \rightarrow thin Cr depletion layer in stainless steel \rightarrow bulk stainless steel. The formation of a very thin Cr_2O_3 bonding layer was consistent with the results from a similar study [1]. However the existence of reduced Cu particles next to Cr_2O_3 was first observed in the current study. It should be emphasized that this type of bonding could occur only in GC-SS seals where an interfacial redox proceeded over the surface reduction of the oxidants in glass-ceramic.

2.3. Pin adhesion test

 SB_100Cu glass-ceramic cubes were placed on to top of stainless steel pins for a GC-pin bonding test. Figures 12a and 12b show a first GC-pin group that was exposed to the N_2 , and a second group that was processed inside graphite fixtures, respectively. The wetting of glass-ceramic in group 1 varied, from a full wetting of pins 1, 2 and 4, to a partial wetting of pin 3, to a non-wetting of pins 5 and 6. No reduced Cu at the surface of the glass-ceramic cubes was observed. For pins 1 through 4, the CuO was primarily reduced for interfacial redox as evidenced by the presence of a thin layer of Cu in the glass-ceramic near the interface. For the non-wetting glass-ceramic cubes on pins 5 and 6, the accumulation of Cu at the contact area was also obvious.

On the other hand, poor wetting of the SB_100Cu glass-ceramic cubes on stainless steel pins was seen in the second group. The CuO was mainly reduced at the glass-ceramic surface as the reflowed glass-ceramic beads appeared to be coated by metallic Cu. There might be a certain level of interfacial redox, as evidenced by the adhesion of glass-ceramic beads to the pins. However, the surface reduction of CuO was clearly the dominant reaction over the interfacial redox.

In pin-GC-pin bonding tests of SB_050 Cu and SB_100Cu glass-ceramics in graphite fixtures, Cu always showed, without exception, on the side wall of disc-shaped glass-ceramic sandwiched between pins. The GC-SS adhesion in these tests was inconsistent. Some glass-ceramics detached from stainless steel pins right out of the furnace. Others were bonded after sealing but could be easily broken off from pins in handling. Inspection of the de-bonded glass-ceramic interfaces showed no or a minimum presence of Cu, indicating the absence of interfacial redox. As a result no study has been performed on the bonding strength on GC-SS samples sealed in graphite fixtures.

The GC-pins specimens 1, 2 and 4 in Figure 12a were selected to measure bonding strength and examine the failure mechanism by pull tests. The glass-ceramic was bonded in to a semi-spherical recess at the center of a diameter 0.500 x thickness 0.125 inch aluminum disc using Henkel Hysol EA9394 2-part epoxy. The assembly was cured at 150 °C for 2 hours with the stainless steel pin being held vertical to the aluminum discs by a fixture. A close view on the GC-pin bonded to aluminum disc is shown in Figure 13a.

Pull tests of the GC-pins 1, 2 and 4 bonded to aluminum were performed by the Romulus Universal Materials Tester. The corresponding breaking forces are shown in Table 1. Two different failure modes were observed. The GC-pin 2 failed at the CG-SS interface with a breaking force around 14,000 Psi, as shown in Figure 13b. GC-pins 1 and 4 failed primarily at the GC-epoxy interface (Figure 13c), along with a failure within epoxy (Figure 13d). All three breaking forces far exceeded the manufacturer specified bonding strength ~ 4000 Psi of the epoxy.

2.4. Bonding mechanism and analysis on fracture interfaces of GC-pin 2 sample

The post-pull test GC-pin 2 specimen was further examined to study the fracture mechanisms (Figures 14a and 14b). The stainless steel surface is mostly covered by residual glass, including large chunks pulled from the glass-ceramic. The machine marks are seen in only a small fraction of the contacted area. The square trace on the stainless steel matches the footprint of the original SB_100Cu glass-ceramic cube that was placed over the stainless steel pin. Accordingly, the fracture glass-ceramic surface shows missing pieces that mirror those on the stainless steel surface. There is also a large area with exposed Cu on the glass-ceramic.

Figure 15 shows the secondary electron (SE) and backscattering electron (BSE) images of the fractures surfaces of the stainless steel and glass-ceramic, taken from the red box in Figure 14a. The stainless steel and glass-ceramic images were coordinated to mirror each other over the center mirror line. Clearly, it appeared the failure cut across the entire interface, from a GC-GC fracture inside the glass-ceramic to fractures that exposed Cr₂O₃, as well as the Cu+GC interfacial layers. An element mapping on the fracture stainless steel surface revealed the

coexistence of: 1) residual glass-ceramic, 2) Cr₂O₃ mixed with a thin layer of glass-ceramic, and 3) end surface of steel pin. Element mapping on the fracture glass-ceramic surface correspondingly revealed: 1) the fractured glass-ceramic, 2) a layer of Cu metallic particles embedded in the glass-ceramic, and 3) Cr₂O₃ mixed with a thin layer of glass-ceramic.

SEM elemental mapping in the red boxed area in Figure 15 captured a junction of three different failure modes. Maps of Cu, Cr, Fe, Si, Al, P, and O across the box at both the fractured glass-ceramic and pin surface with mirror symmetry are shown in Figure 16. Close inspection of the presence and distribution of each element around the junction, combining with the correlation of elements over the mirrored glass-ceramic and pin fractured surfaces, provided a base to identify several failure mechanisms.

Figure 17 summarizes three failure modes: 1) The area marked as Cr₂O₃ represented the break off of the interfacial Cr₂O₃ bonding layer from the stainless steel. The failure mode is Cr₂O₃-SS.

2) The area marked as Cu showed a high density of Cu particles and represented a break off of the Cu + GC from the interfacial Cr₂O₃ bonding layer. The failure mode is Cu/GC- Cr₂O₃. 3) The area marked GC is very much into the bulk glass-ceramic, representing a break off of the glass-ceramic itself. The failure mode is GC-GC.

It is evident that a strong interfacial bond was established between the stainless steel pin and SB_100Cu glass-ceramic, provided that the GC-SS was processed in the presence of trace oxygen which drove the CuO in the glass-ceramic towards the interface for redox. A strong joint between such glass-ceramic and stainless steel is possible, when a graphite fixture and the

associated reducing atmosphere do not present. However, for GCtSS seals where a graphite fixture is used, the CuO modified glass-ceramics are not suitable, mainly because of the preference of surface reduction over the interfacial redox reaction of the CuO.

Conclusions

The CoO modified glass-ceramics were promising in terms of adhesion to stainless steel. Redox of CoO at the GC-SS interface and strong bonding of glass-ceramic to stainless steel were observed. However, low mobility of Co⁺⁺ ions in the glass-ceramics limited the amount of CoO for redox. There is no distinct thin continuous Cr₂O₃ interfacial bonding layer, despite the existence of discrete Cr₂O₃ crystals at the interface. A reaction zone in glass-ceramic with P depletion still existed, so did the abnormal crystal growth in the reaction zone.

For CuO modified glass-ceramics, a strong bonding between glass-ceramic and stainless steel was achieved when the samples were processed in the presence of trace oxygen. The CuO in glass-ceramics was reduced at the GC-SS interface for redox to form metallic Cu particles and an interface Cr₂O₃ bonding layer. Pull tests suggested multiple failure modes in these well bonded GC-SS specimens. On the other hand, the CuO was reduced at the glass-ceramic surface when the specimens were processed in graphite fixtures with a local reducing atmosphere. The interface bonding was not established due to the absence of interfacial redox. The glass-ceramics with CuO are good candidates for strong GC-SS joining where no graphite fixture is required. The bonding of CuO modified glass-ceramics to stainless steel using alternative fixture

materials, for example, boron nitride where a local reducing atmosphere does not present, is worth further investigation.

Acknowledgement

The authors would like to thank Mrs. Bonnie McKenzie for SEM characterization, Dr. Ping Lu for TEM analysis and Dr. Don Susan for insightful discussions on GC-SS interactions. This work was supported by the Laboratory Directed Research and Development program at Sandia National Laboratories, a multi-program laboratory managed and operated by Sandia Corporation, a wholly owned subsidiary of Lockheed Martin Corporation, for the U.S. Department of Energy's National Nuclear Security Administration under contract DE-AC04-94AL85000.

References

- 1 Donald I. Glass-to-Metal Seals. Society of Glass Technology; 2009.
- 2 Henderson WR, Kramer DP, Sullenger DB. Determinination of the Optimum Crystallization Conditions of a High Thermal Expansion Glass-Ceramic. Miamiaburg, OH: Monsanto Research Corp; 1984 Monsanto Research Corp. MLM-3136.
- 3 Loehman RE, Headley TJ. Design of High Thermal Expansion Glass-Ceramcis. In: Pask JA, Evans AG, editors. Ceramic Microstructure'86; 1987. p. 33-43.
- 4 McCollister HL, Reed ST, inventors. Glass Ceramic Seals to Inconel. 1983. US4414282.
- 5 Reed S, Stone RG, McCollister HL, Wengert PR, inventors. Method of Processing "BPS" Glass Ceramic and Seals Made Therewith. 1998 Nov. US5820989.
- 6 Donald IW. Preparation, Properties and Chemistry of Glass- and Glass-ceramic-to-metal Seals and Coating. Journal of Matrials Science. 1993;28:2841-2886.
- 7 Knorovsky GA, Brow RK, Watkins RD, Loehman RE. Interfacial Debonding in Stainless Steel/Glass Ceramic Seals. Albuquerque: Sandia National Laboratories; 1989. SAND89-1866C.
- 8 Loehman RE. Interfacial Reaction in Ceramic-Metal Systems. Ceramic Bulletin. 1989;68(4):891-896.
- 9 Watkins RD, Loehman RE. Interfacial Reaction Between a Complex Lithium Silicate Glass-Ceramic to Metal Seals. Advanced Ceramic Materials. 1986;1(1):77-80.
- 10 Kunz SC, Loehman RE. Thermal Expansion Mismatch Produced by Interfacial Reactions in Glass-Ceramic to Metal Seals. Advanced Ceramic Mateirals. 1986;2(1):69-73.
- 11 Benisu M, Brow RK, White JE. Interfacial Reaction Between Lithium Silicate Glass-Ceramics and Ni-Based Superalloys and the Effect of Heat Treatment at Elevated Temperatures. Journal of Materials Science. 2004 505-518.
- 12 Susan DF, Van Den Avyle JA, Monroe SL, Sorensen NR, McKenzie BB, Christensen JE. The Effects of Pre-Oxidation and Alloy Chemistry of Austenitic Stainless Steels on Glass/Metal Sealing. Oxidation of Metals. 2009;73(1-2):311-335.
- 13 Susan DF, Knorovsky GA, Robino CV, Michael JR, Rodriguez MA, Perricone MJ. Surface alloy depletion and martensite formation during glass to metal joining of austenitic stainless steels. Science and Technology of Welding and Joining. 2012;17(4):321-332.

List of Tables

Table 1. Bonding Strength and Failure Mode of GC-pin 1, 2 and 4.

Figure Captions

- Figure 1. Sessile drop of CoO doped glass-ceramics on SS. a) SB_Co1, and b) SB_Co2, c) Elan46, BPS_Co1 and BPS_Co2, and d) High magnification view of BPS_Co1 and BPS_Co2 in c).
- Figure 2. GC-pin tests inside graphite fixtures. a) BPS_Co1, b) BPS_Co2, and c) transmission optical view highlighting the Co depletion zone in BPS_Co2 near stainless steel pin.
- Figure 3. (a) Bonded and fractured pin-GC-pin samples using BPS_Co2 glass-ceramic, (b) cross section of glass-ceramics in sample 2, and (c) cross section of glass-ceramic and pin surfaces of sample 3.
- Figure 4. SEM images and element mapping of BPS Co2 glass-ceramic and SS pin interface.
- Figure 5. Sessile drop test SB_0125CU, SB_050Cu, SB_075 Cu and SB_100Cu glass-ceramics.
- Figure 6. Sessile drop test of SB_050Cu and SB_100 Cu glass-ceramics inside a graphite box on (a) as machined and (b) pre-oxidized stainless steel coupons.
- Figure 7. SEM image and element maps of SB_100Cu sessile drop specimen on stainless steel.
- Figure 8. SEM images and P map in bulk glass-ceramic and near the GC-SS interface.
- Figure 9. TEM image and element mapping of SB 100Cu GC-SS interface.
- Figure 10. SAED patterns from different parts of the SB_100Cu BC-SS interface for phase identification.
- Figure 11. Illustration of GC-SS bonding from interfacial redox.
- Figure 12. Pin-SB_100Cu glass-ceramic adhesion tests in different local atmosphere. (a) Exposed to the furnace N₂, and (2) covered in graphite fixture.
- Figure 13. (a) GC-pin bonded to Al substrate, (b) GC-pin 2 failed at the GC-pin interface. GC-pins 1 and 4 failed at epoxy-GC interface, (c) failed epoxy and (d) glass-ceramic surfaces.
- Figure 14. Optical images of a) the fractured surfaces of stainless steel pin and b) glass-ceramic from GC-pin 2.
- Figure 15. Mirrored SE and BSE images of the fractured surfaces of stainless steel pin and glass-ceramic from GC-pin 2.

- Figure 16. Mirrored SEM element maps of fractured SB100Cu glass-ceramic and stainless steel pin surfaces.
- Figure 17. Mirrored BSE images on stainless steel pin and glass0ceramic with marked multiple failure modes.

Table 1. Bonding Strength and Failure Mode of GC-pin 1, 2 and 4.

GC-pin	Bonding strength		Failure mode
	lb	~ Psi	
1	53	6750	GC-epoxy interface + epoxy
2	110	14000	GC-SS pin interface
4	66	8400	GC-epoxy interface + epoxy

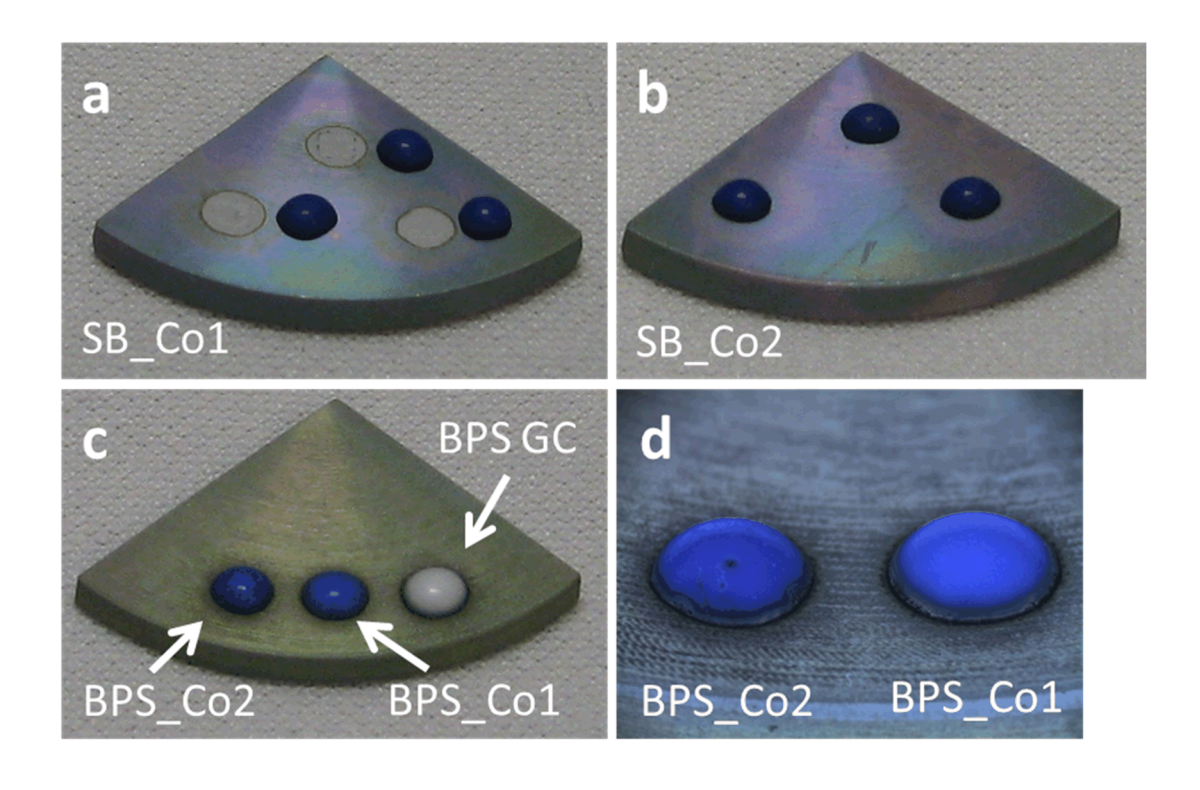


Figure 1. Sessile drop of CoO doped glass-ceramics on SS. a) SB_Co1, and b) SB_Co2, c) Elan46, BPS_Co1 and BPS_Co2, and d) High magnification view of BPS_Co1 and BPS_Co2 in c).

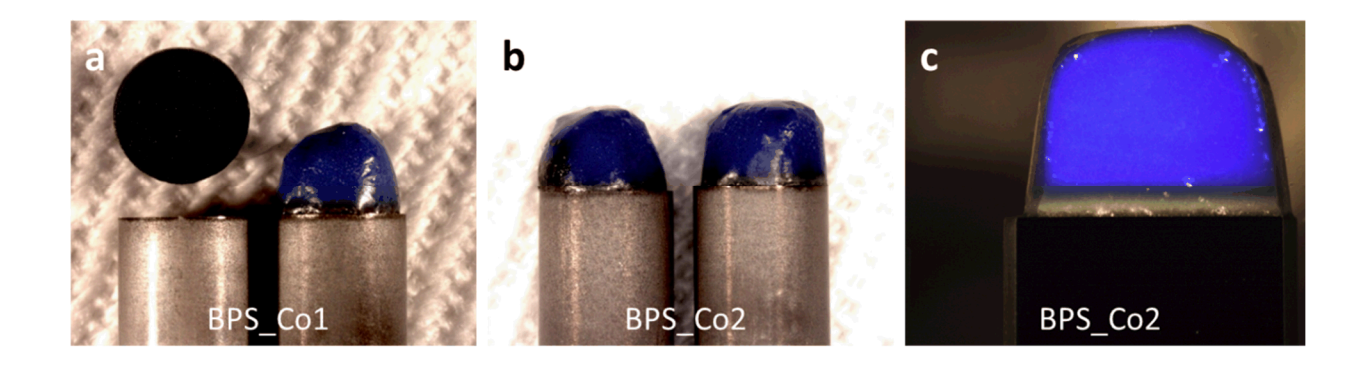


Figure 2. GC-pin tests inside graphite fixtures. a) BPS_Co1, b) BPS_Co2, and c) transmission optical view highlighting the Co depletion zone in BPS_Co2 near stainless steel pin.



Figure 3. (a) Bonded and fractured pin-GC-pin samples using BPS_Co2 glass-ceramic, (b) cross section of glass-ceramics in sample 2, and (c) cross section of glass-ceramic and pin surfaces of sample 3.

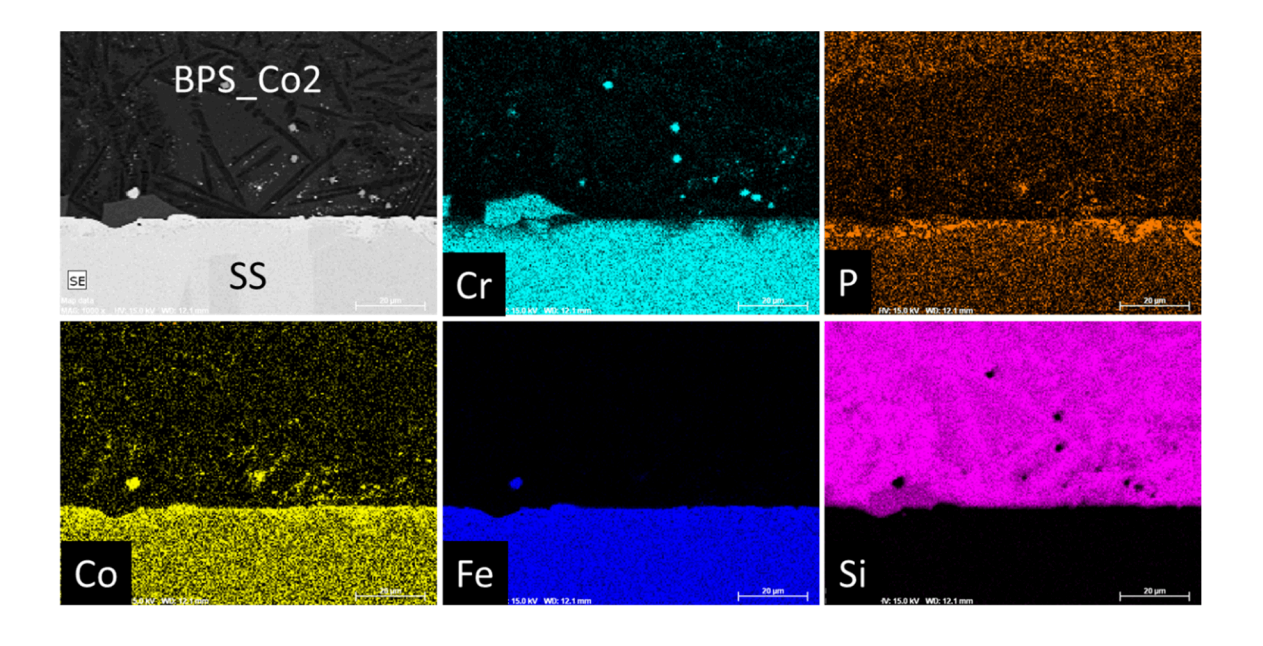


Figure 4. SEM images and element mapping of BPS_Co2 glass-ceramic and SS pin interface.

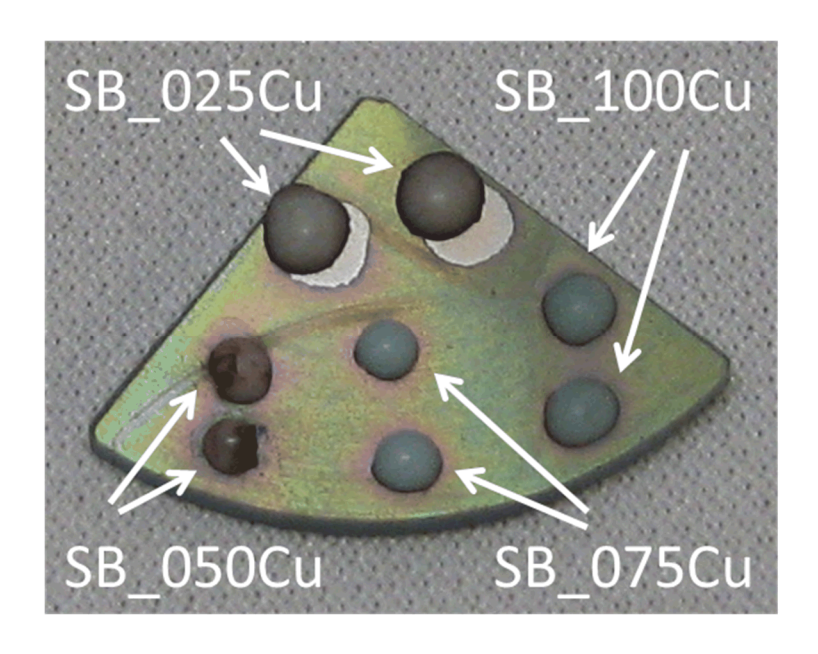


Figure 5. Sessile drop test SB_0125CU, SB_050Cu, SB_075 Cu and SB_100Cu glass-ceramics.

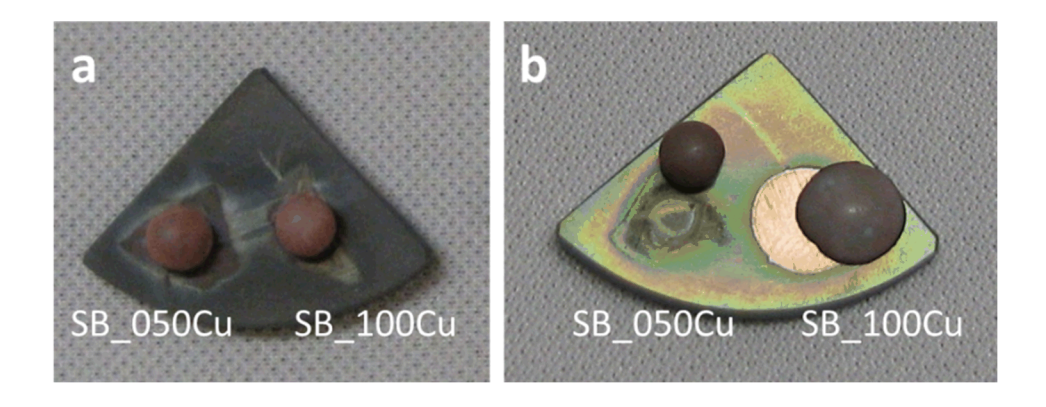


Figure 6. Sessile drop test of SB_050Cu and SB_100 Cu glass-ceramics inside a graphite box on (a) as machined and (b) pre-oxidized stainless steel coupons.

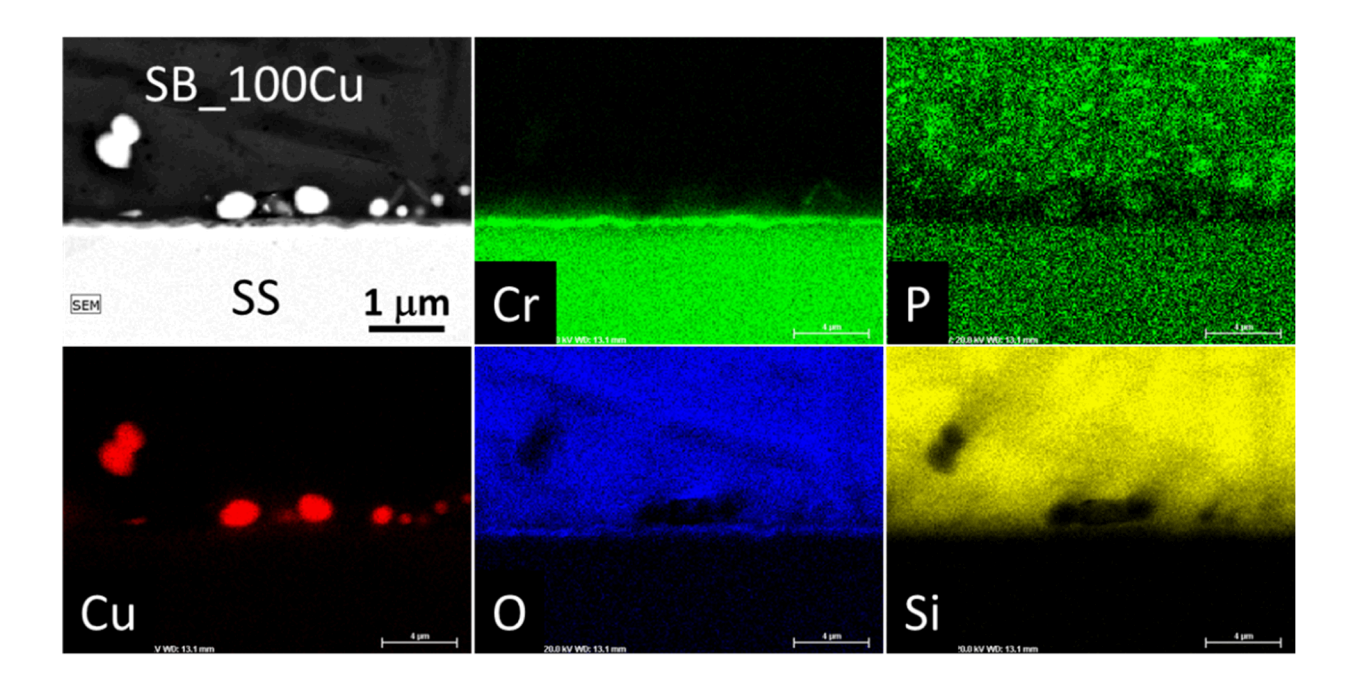


Figure 7. SEM image and element maps of SB_100Cu sessile drop specimen on stainless steel.

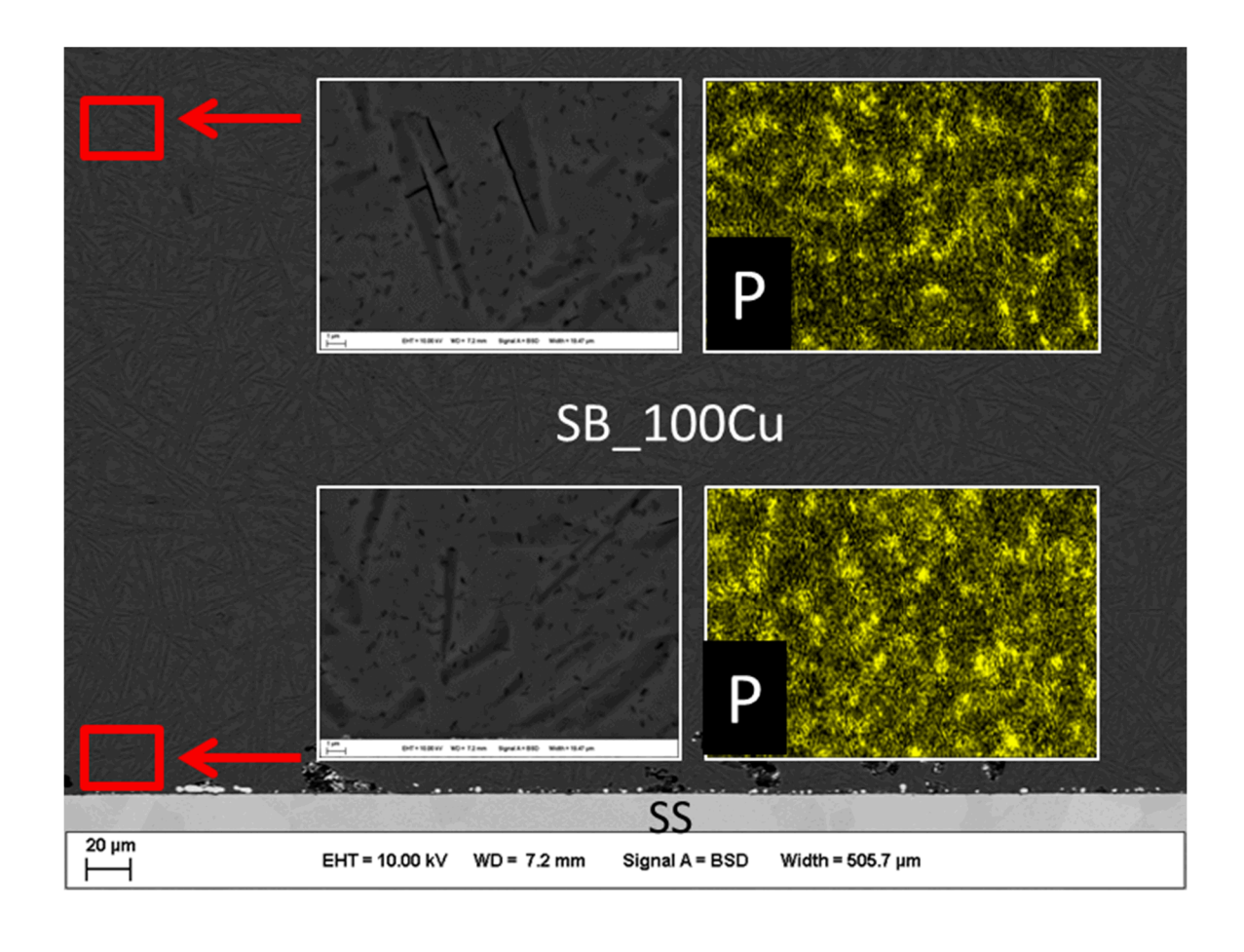


Figure 8. SEM images and P map in bulk glass-ceramic and near the GC-SS interface.

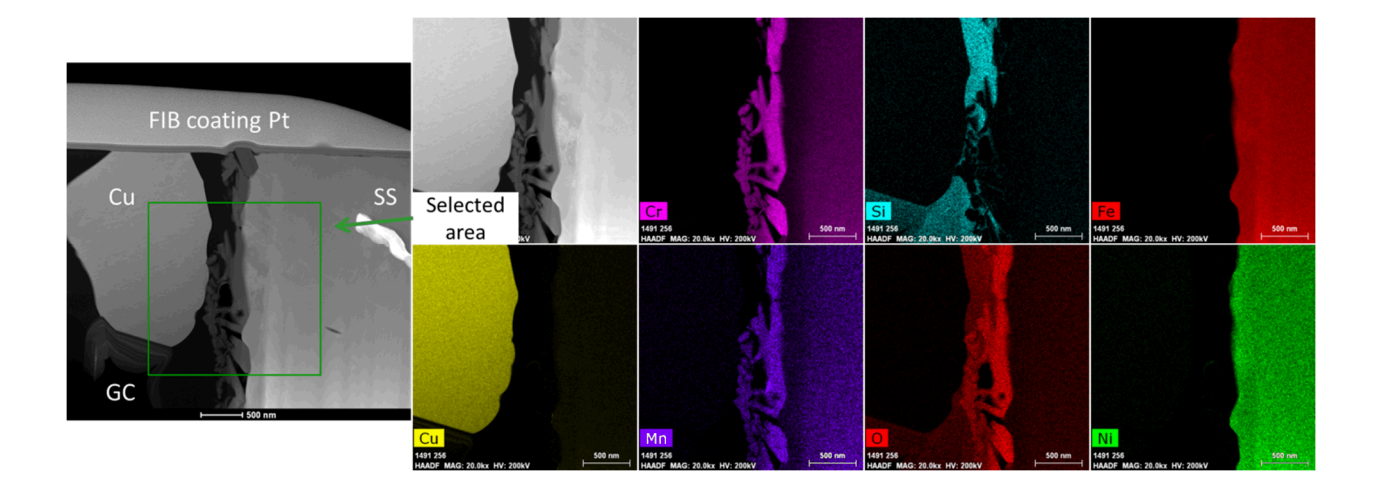


Figure 9. TEM image and element mapping of SB_100Cu GC-SS interface.

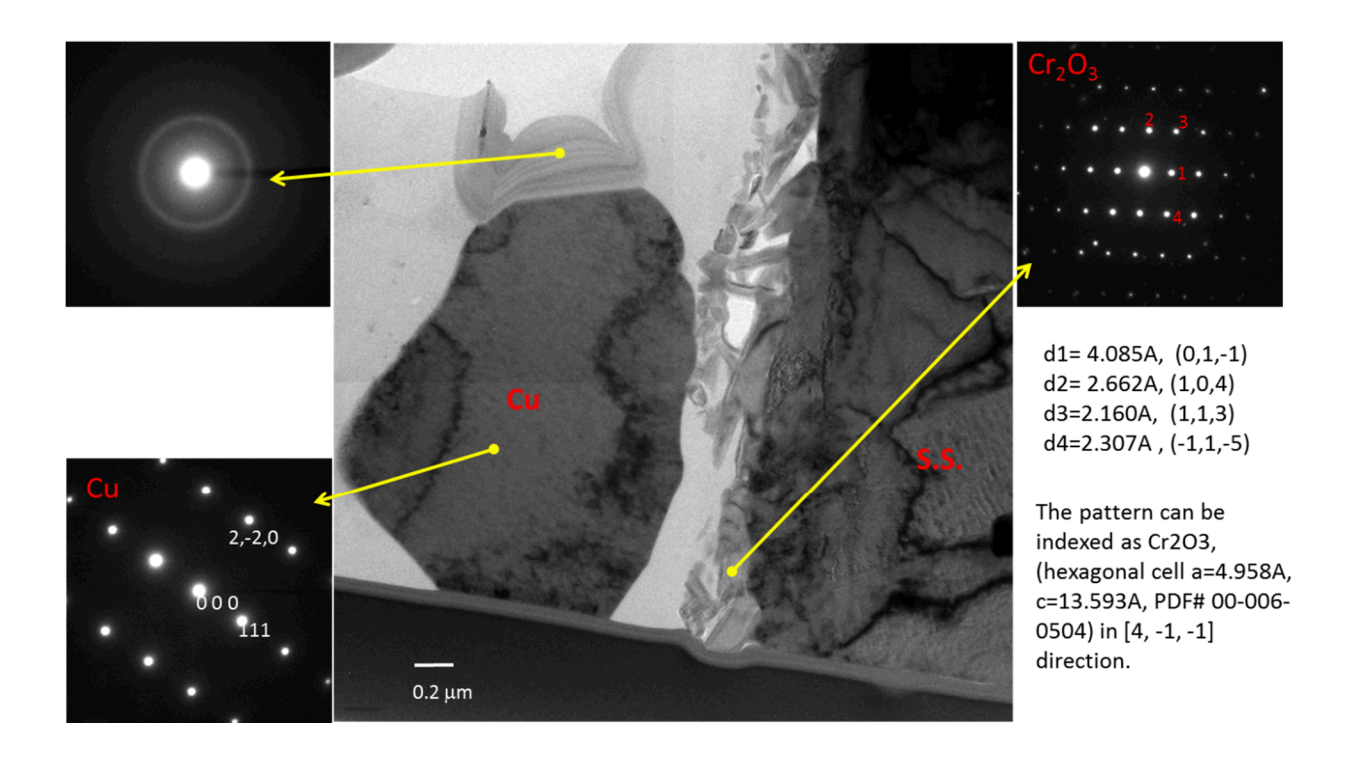


Figure 10. SAED patterns from different parts of the SB_100Cu BC-SS interface for phase identification.

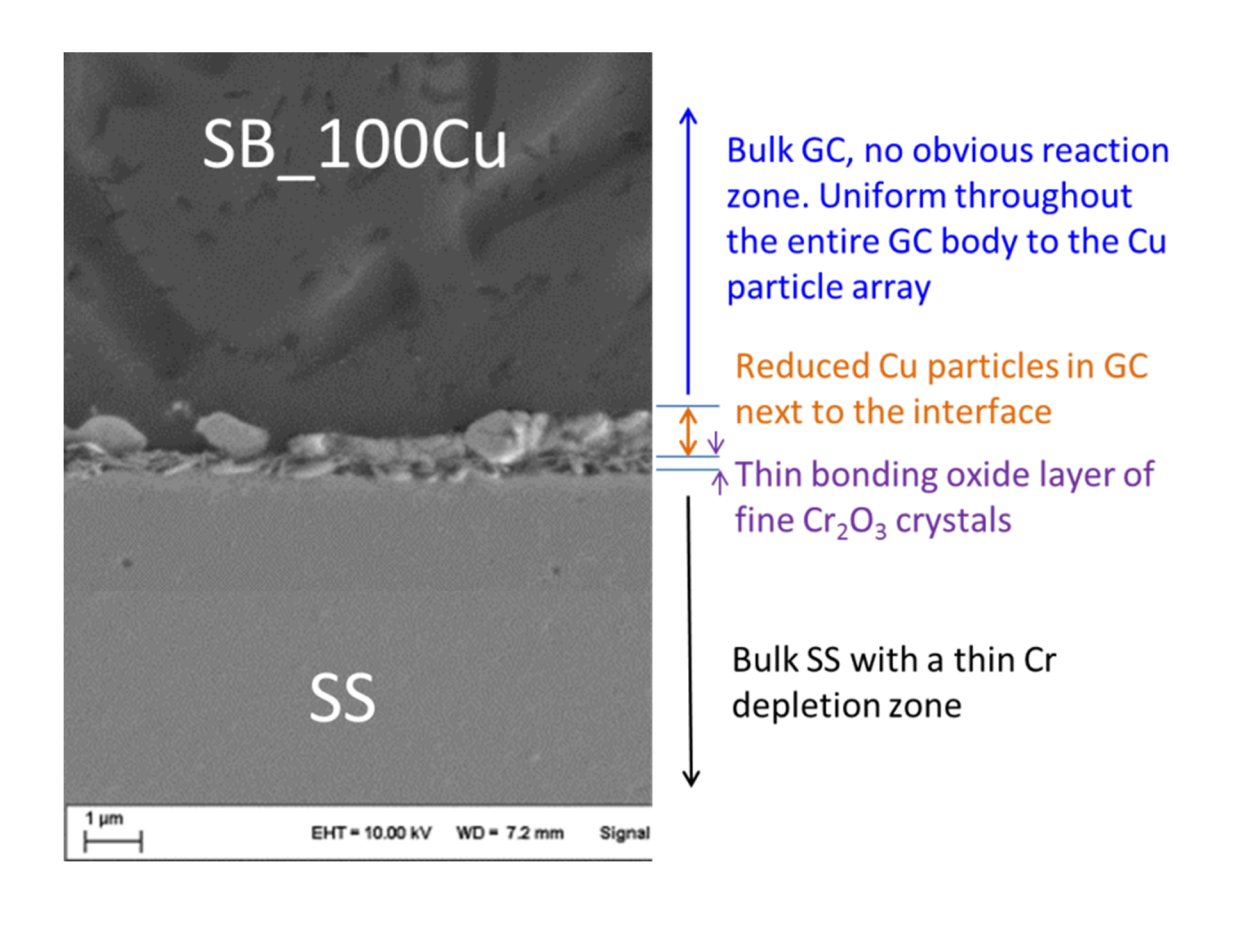


Figure 11. Illustration of GC-SS bonding from interfacial redox.

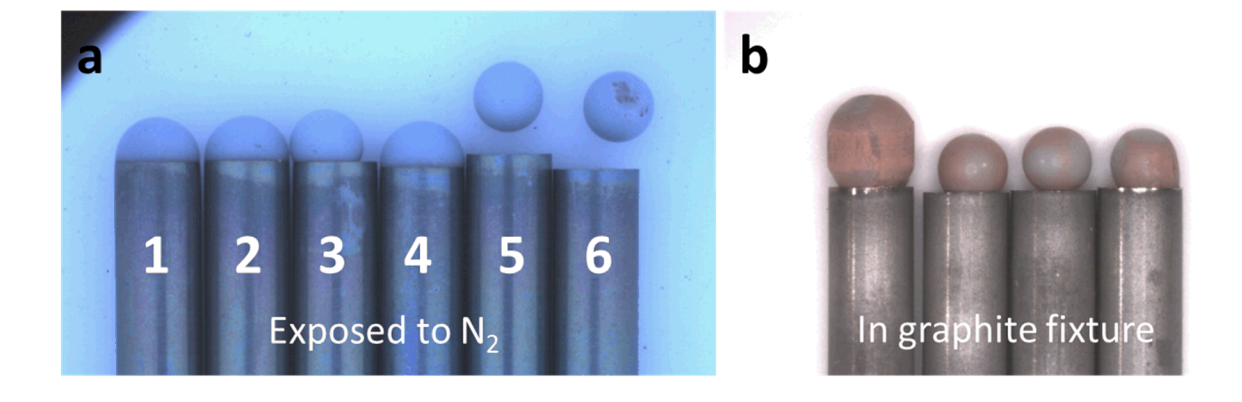


Figure 12. Pin-SB_100Cu glass-ceramic adhesion tests in different local atmosphere. (a) Exposed to the furnace N_2 , and (2) covered in graphite fixture.

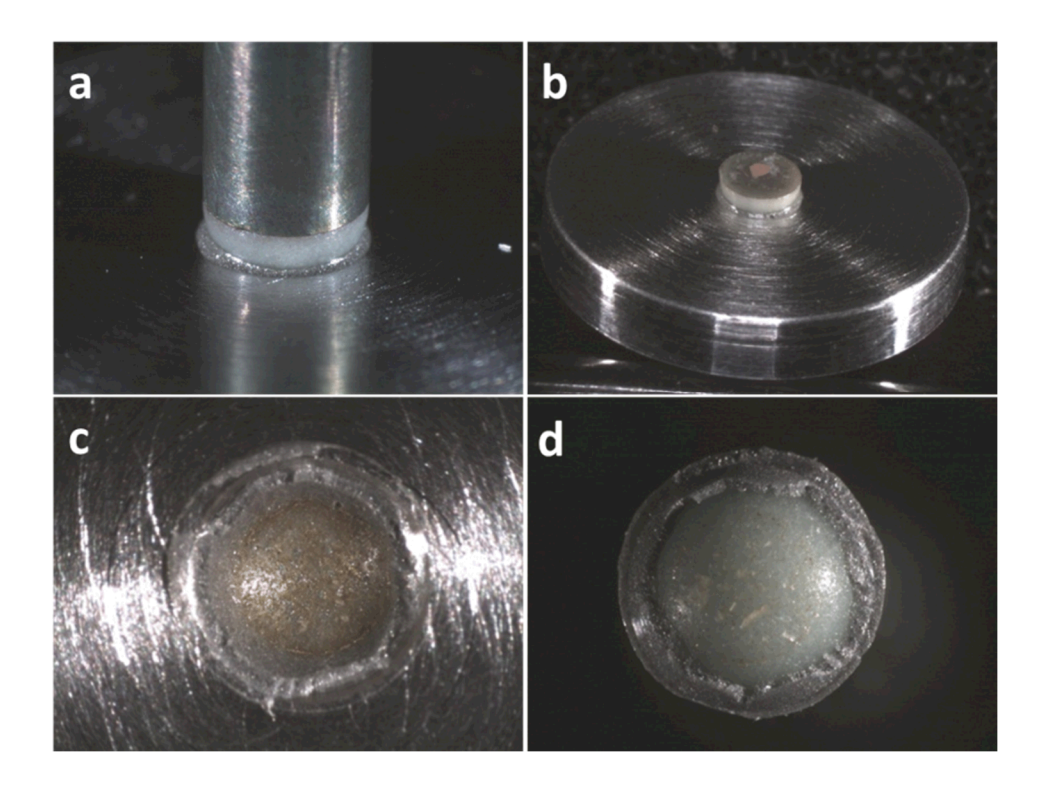


Figure 13. (a) GC-pin bonded to Al substrate, (b) GC-pin 2 failed at the GC-pin interface. GC-pins 1 and 4 failed at epoxy-GC interface, (c) failed epoxy and (d) glass-ceramic surfaces.

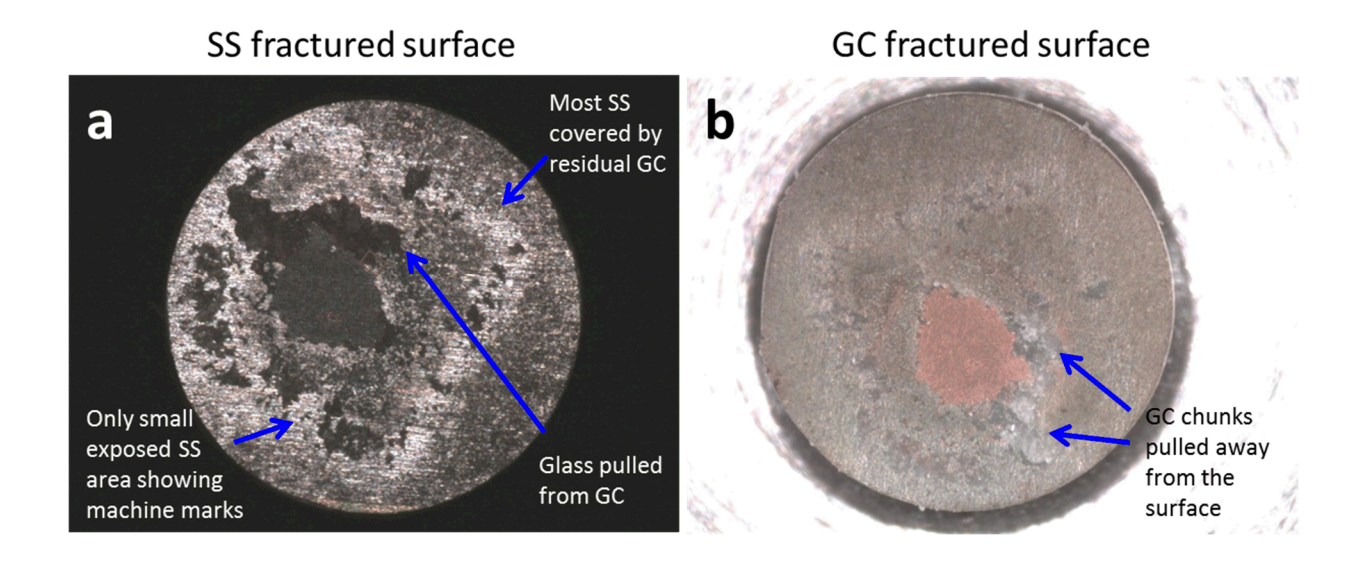


Figure 14. Optical images of a) the fractured surfaces of stainless steel pin and b) glass-ceramic from GC-pin 2.

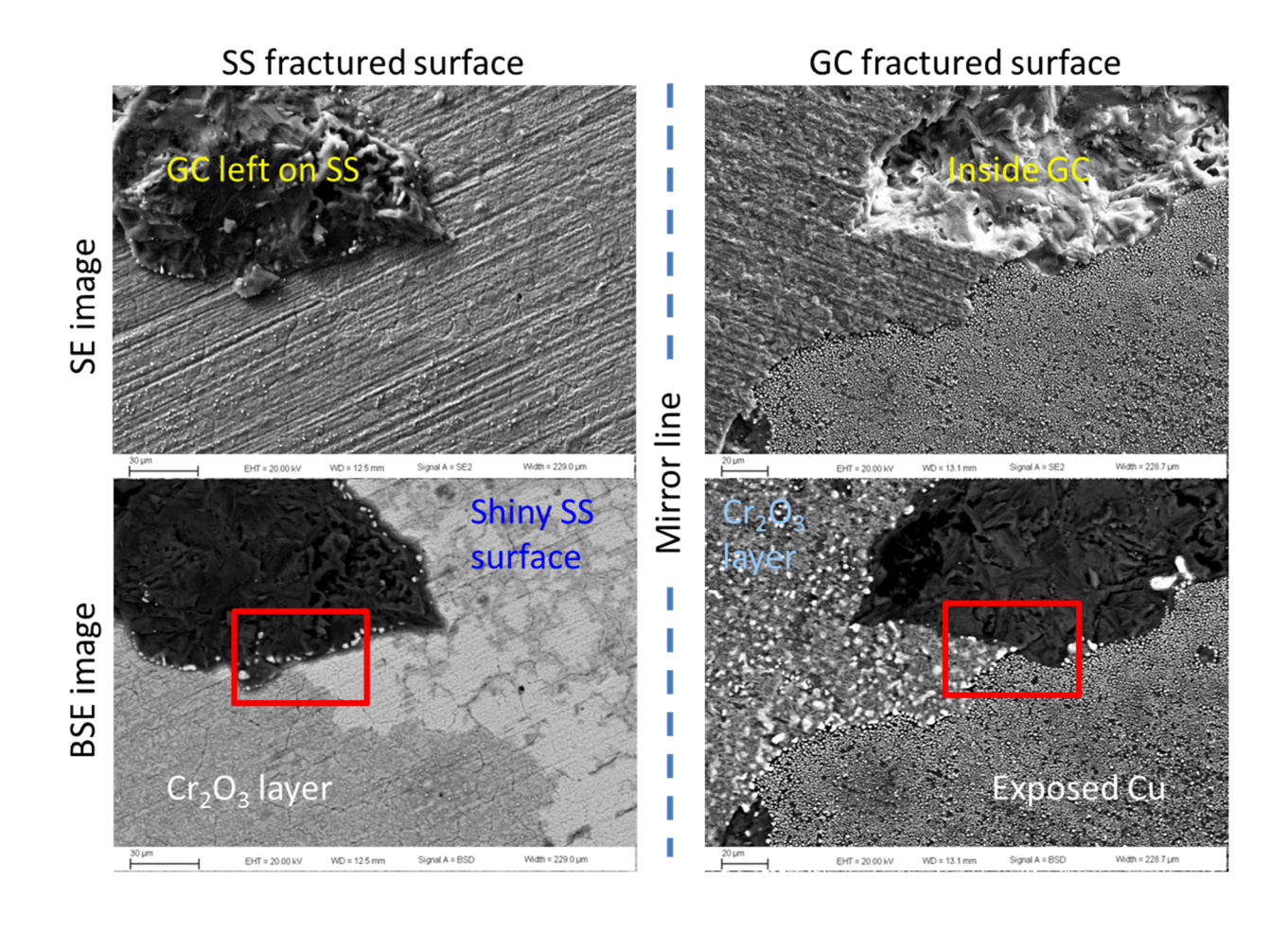


Figure 15. Mirrored SE and BSE images of the fractured surfaces of stainless steel pin and glass-ceramic from GC-pin 2.

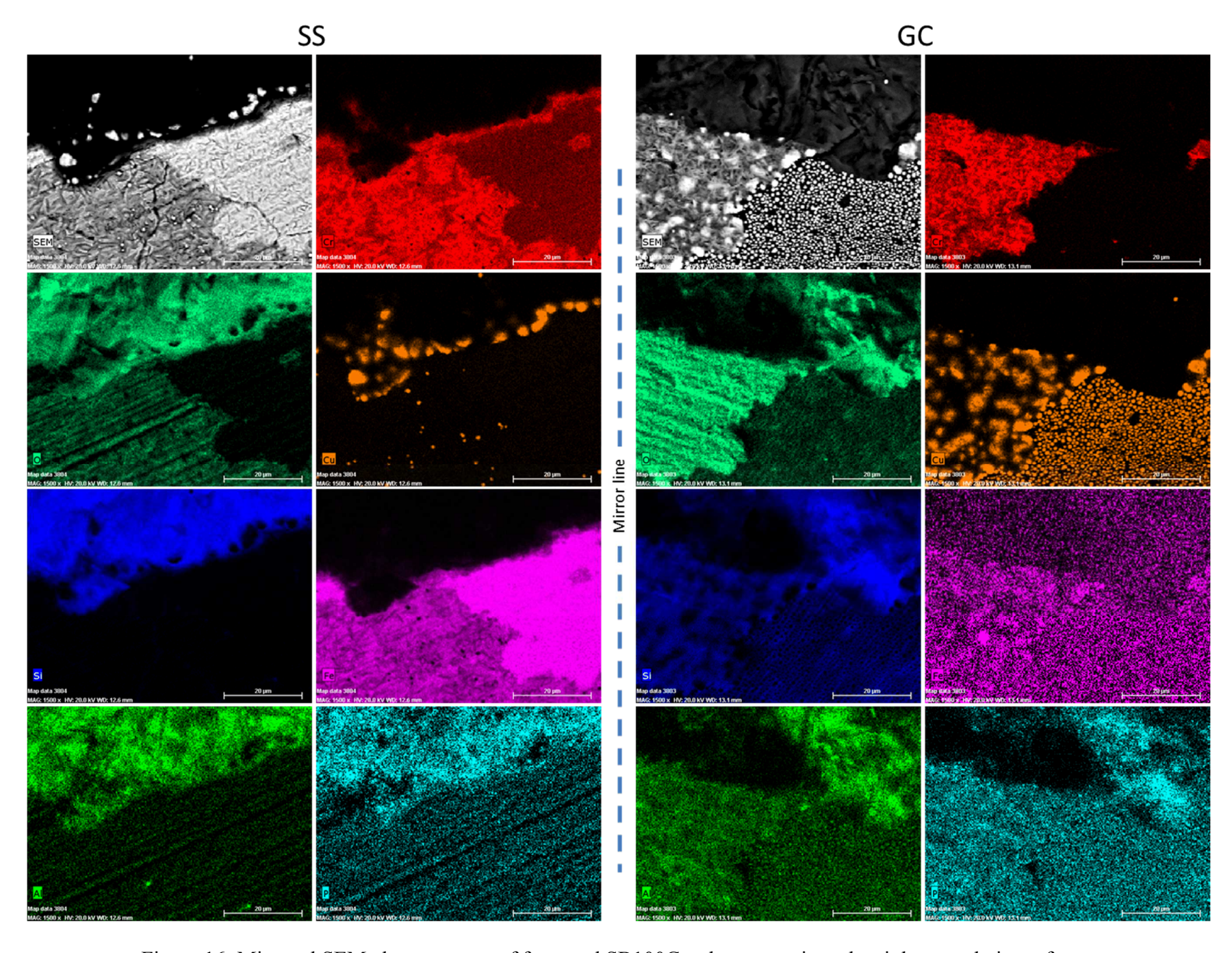


Figure 16. Mirrored SEM element maps of fractured SB100Cu glass-ceramic and stainless steel pin surfaces.

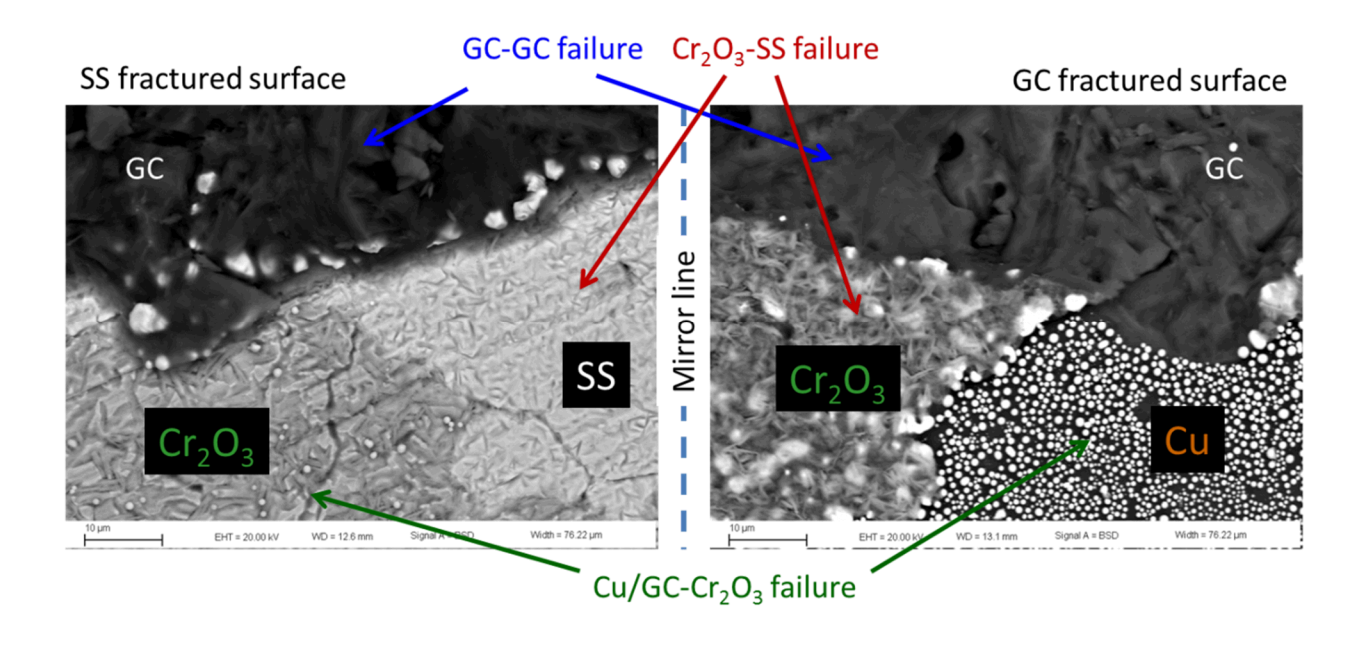


Figure 17. Mirrored BSE images on stainless steel pin and glass0ceramic with marked multiple failure modes.